第 48 卷 第 5 期/2021 年 3 月/中国激光 研究论文

中国激光

1645 nm 单频脉冲 Er∶YAG 陶瓷激光器

宋睿，李尚桦，陈朝勇，王庆，高明伟，高春清*

北京理工大学光电学院光电成像技术与系统教育部重点实验室，北京 100081

摘要 设计和研制了 1645 nm Er∶YAG 单频脉冲激光器系统，采用注入种子技术和对称泵浦的双 Er∶YAG 陶瓷结构，当脉冲重复频率为 200 Hz 时，获得了最大平均脉冲能量为 22.75 mJ、脉冲宽度为 223.1 ns 的单频调 Q 脉冲激光输出，x 和 y 方向上的光束质量因子分别为 1.16 和 1.15，0.5 h 内单频脉冲的中心频率稳定性为 578 kHz，激光脉冲输出能量的不稳定性小于 0.5%。

关键词 激光器；全固态激光器；注入锁定；大能量；单频；激光陶瓷

中图分类号 TN248 **文献标志码** A **doi**：10.3788/CJL202148.0501012

1 引 言

稳定可靠的单频、大能量人眼安全激光器是激光雷达及相干探测的重要光源[1-4]。目前，国内外已经有很多研究成果报道了人眼安全的 1645 nm 单频脉冲激光输出[5-7]。2015 年，哈尔滨工业大学采用种子光注入蝶形谐振腔的方案，在 100 Hz 的重复频率下获得了能量为 2.9 mJ 的单频激光脉冲，脉冲宽度为 160 ns[8]。2018 年，美国 Fibertek 公司研制了用于差分吸收雷达的 Er∶YAG 单频激光器，获得了最大脉冲能量为 6 mJ、重复频率为 1 kHz、脉宽为 120 ns 的激光输出[9]。2019 年，北京理工大学研制了双波长混合泵浦双 Er∶YAG 晶体的注入锁定脉冲激光器，当重复频率分别为 200，300，500 Hz 时获得了能量为 20.3，16.87，12.84 mJ 的单频脉冲，对应的脉冲宽度分别为 110，125，162 ns[10]。与晶体材料相比，陶瓷材料具有生长时间短、可大规模生产和掺杂浓度灵活等优点[11-12]。因此，Er∶YAG 陶瓷材料也常被用于制备 1.6 μm 激光器[13-14]。

本文报道了我们研制的单频脉冲 Er∶YAG 陶瓷激光器工程化样机，该研究进一步减小了激光器的体积，提高了单频激光频率的稳定性。与我们先前报道的工作[15]相比，Er∶YAG 激光器样机的体积缩小了一半，单频激光频率的稳定性提升了两倍。激光器体积的缩小限制了操作空间，增大了谐振腔调节以及模式匹配的难度，特别是在长腔、大能量、对频率稳定性要求高的激光系统中。为了避免有限空间引起的性能降低，我们以对称泵浦的双 Er∶YAG 陶瓷结构，获得了脉冲最大平均能量为 22.75 mJ、脉冲宽度为 223.1 ns、光束质量接近衍射极限的 1645 nm 单频调 Q 激光输出，单频脉冲的中心频率稳定性提高到了 578 kHz，脉冲能量的不稳定性小于 0.5%，输出的单频脉冲激光在 x 和 y 方向上的光束质量因子分别为 1.16 和 1.15。

2 系统结构

注入锁定的单频 Er∶YAG 脉冲激光系统的结构原理图如图 1 所示。整体系统主要包括三部分：1）Er∶YAG 种子激光器；2）对称泵浦的双 Er∶YAG 陶瓷环形腔从动激光器；3）探测及注入锁定控制系统。为了提高模式匹配效率并缩小激光器体积，从动激光器的腔型设计采用全反镜多次折叠的方案。

2.1 种子激光器

为了提升脉冲激光的稳定性，种子源采用了单频连续 Er∶YAG 非平面环形腔（NPRO）激光器。Er∶YAG 的掺杂浓度（原子数分数，全文同）为

收稿日期：2020-10-26；**修回日期**：2020-11-20；**录用日期**：2020-12-08

基金项目：科技部重点研发计划（2017YFB0405203）

* **E-mail**：gao@bit.edu.cn

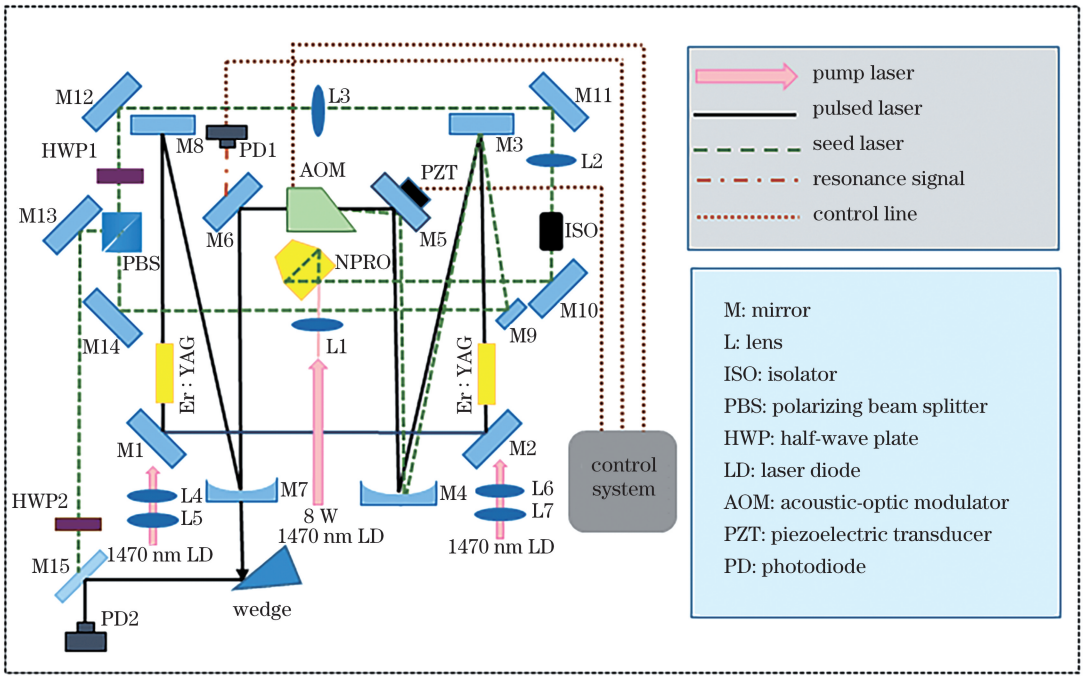

图 1　Er∶YAG 单频脉冲激光系统的原理图

Fig. 1　Principle diagram of Er∶YAG single-frequency pulsed laser system

0.5%，泵浦光入射面与激光出射面为同一平面[16]。种子激光器由一个 1470 nm 的半导体激光器（LD）泵浦，偏振分束器（PBS）将输出的种子激光进行分束，利用声光调制器（AOM）的第一衍射级将 p 偏振光注入到从动激光器中以实现种子注入，s 偏振光用作外差拍频探测的参考光。半波片 HWP1 在 PBS 前调节两路种子光的强度分布比，半波片 HWP2 用于实现拍频种子光的偏振态调节。单频激光的中心波长为 1645.22 nm，输出线宽为 8 kHz。

2.2　脉冲从动激光器

脉冲从动激光器为双 LD 泵浦双 Er∶YAG 陶瓷的对称结构。泵浦源为 1470 nm 的 LD，两束泵浦光分别经过模式匹配透镜耦合系统并聚焦于增益介质中心。为了获得足够的增益并降低上能级转换效应的影响，增益介质采用两个掺杂浓度为 0.25%，体积为 4 mm×60 mm 的 Er∶YAG 陶瓷棒。陶瓷棒的两端均进行了抛光并镀有对泵浦光和激光波段高透的介质膜。为了降低热效应对输出性能的影响，利用半导体制冷器（TEC）将 Er∶YAG 陶瓷棒的温度控制在 18 ℃。

为了同时满足激光雷达对脉冲能量和脉宽的需求，从动谐振腔的总腔长为 2.3 m，并采用结构对称的八镜环形腔。利用多个折叠镜，将谐振腔的长度和宽度缩小，并在中心位置处为种子激光器预留空间，实现空间的合理利用，从而压缩整体系统的体积。M1 和 M2 为 45°泵浦输入镜，表面镀有对 1645 nm 高反、1470 nm 高透的介质膜；M3 和 M8 为对激光波段高反、泵浦光高透的平面镜；M4 与 M7 为凹面镜，其中 M4 表面镀有 1645 nm 的高反膜（反射率＞99%），M7 表面的介质膜对激光的透过率为 20%，有利于激光输出。M5 和 M6 为对 1470 nm 高透、1645 nm 高反的 45°双色镜，其中 M5 的后表面装有压电陶瓷（PZT），用于注入锁定过程中的腔长扫描。

种子注入及激光输出的工作过程如下：p 偏振的种子光通过注入镜 M9 反射进入到从动谐振腔中，调节 M9 的角度，使注入的种子光与 AOM 第一衍射级同路，从而在从动激光器中实现谐振，此时 AOM 处于关断状态。光电探测器（PD1）放置于 M6 后，接收泄漏的谐振信号，并将其传递至控制系统中。同时控制系统在 PZT 上加载三角波，使其持续扫描腔长。当扫描至谐振信号的峰值处且谐振腔的长度满足种子激光频率的相长干涉条件时，终止 AOM 的关断状态，同时腔内出现激光脉冲并输出。

实验采用了外差拍频的方式测试输出脉冲激光的单频特性，输出的脉冲激光经楔形镜分光后，与种子光在 M15 处拍频。M15 为未镀膜镜片，可以充分衰减反射的脉冲激光，使拍频的两路光强度相近。利用光电探测器（PD2）探测拍频信号，并将其传递到示波器中显示。

3 理论分析

注入锁定单频激光器的种子注入实质上是注入的种子光与自发辐射生成的自然光对反转粒子数的竞争，竞争的结果取决于注入的种子光与自然光对反转粒子数的提取速率。影响注入锁定效果的因素有很多，包括注入种子光与谐振光的耦合、注入种子光的频率失谐量和注入种子光的能量等。

注入种子光的能量和频率失谐量对注入锁定结果的影响可以通过求解速率方程来进行模拟仿真。描述从动激光器瞬时电场的基础方程[17]表示为

$$\frac{\mathrm{d}E_n}{\mathrm{d}t}=m(t)\left[E_n+\frac{E_{n0}}{\mathrm{e}^{m(t)\tau_r}-1}\right], \tag{1}$$

$$m(t)=\frac{1}{2}\left[\frac{l}{L}\sigma c\Delta N(t)-\frac{1}{\tau_c}\right]-\mathrm{j}\Delta\omega, \tag{2}$$

式中：$E_n(n=1,2)$为从动激光器的瞬时电场，E_1 表示注入种子光后的瞬时电场，E_2 表示自发辐射噪声中起振的瞬时电场；$E_{n0}(n=1,2)$表示注入种子光的电场($n=1$)及自发辐射噪声的电场($n=2$)；$m(t)$表征从动激光器谐振腔对电场的增强作用；σ 为增益介质的发射截面；c 为真空中的光速；ΔN 为反转粒子数；τ_c 为光子衰减时间；τ_r 为光子在腔内的往返时间；$\Delta\omega$ 为种子光频率与从动激光器中的谐振模式频率(最接近种子光频率)的频率差，当从动激光器在自发辐射噪声中起振时，此项为零。

由自由振荡激光器的速率方程可以得到反转粒子数与光子数的关系[18]，即

$$\frac{\mathrm{d}\Delta N(r,t)}{\mathrm{d}t}=-\gamma\sigma c\Phi(r,t)\Delta N(r,t), \tag{3}$$

式中：r 为径向距离；γ 为反转因子；Φ 为随时间变化的腔内光子数。

假定泵浦光及激光均为高斯分布，则有

$$\Delta N(r,t)=\Delta N(0,t)\exp(-2r^2/\omega_p^2), \tag{4}$$

$$\Phi(r,t)=\Phi(0,t)\exp(-2r^2/\omega_l^2), \tag{5}$$

式中：ω_p 和 ω_l 分别为泵浦光束和激光光束在增益介质中心处的束腰半径。将(4)、(5)式代入到(3)式中，并进行积分得到

$$\frac{\mathrm{d}\Delta N(0,t)}{\mathrm{d}t}\int_0^\infty\exp(-2r^2/\omega_p^2)\cdot 2\pi r\,\mathrm{d}r=-\gamma\sigma c\Phi(0,t)\Delta N(0,t)\times\int_0^\infty\exp(-2r^2/\omega_p^2)\exp(-2r^2/\omega_l^2)\cdot 2\pi r\,\mathrm{d}r, \tag{6}$$

将 $\Delta N(0,t)$和 $\Phi(0,t)$分别表示为时间 t 的函数，即 $\Delta N(t)$和 $\Phi(t)$，得到

$$\frac{\mathrm{d}\Delta N(t)}{\mathrm{d}t}=\frac{-\gamma\sigma c\omega_l^2}{\omega_l^2+\omega_p^2}\Phi(t)\Delta N(t)。 \tag{7}$$

当完成种子注入后，可以认为腔内的光子数包括两部分：在种子光的基础上增长的光子和由于自发辐射在噪声中增长的光子。将两部分求和，可得到腔内总光子数[19]：

$$\Phi(t)=\frac{\varepsilon}{h\nu}\left[E_1^2(t)+E_2^2(t)\right], \tag{8}$$

式中：ε 为介质的介电常数；h 为普朗克常量；ν 为频率。

利用(1)、(7)、(8)式求数值解，并代入实验所用的腔长、增益介质长度以及 Er∶YAG 陶瓷发射截面等参数，可以得到光子数随时间变化的关系。求解过程中所用的初值条件为

$$\frac{\mathrm{d}E_1(0)}{\mathrm{d}t}=\frac{\mathrm{d}E_2(0)}{\mathrm{d}t}=0。 \tag{9}$$

图 2(a)、(b)所示分别为不同的注入种子功率和不同的频率失谐量下的仿真结果。有效的注入锁定意味着在注入种子光基础上增长的模式优先于在受激辐射噪声上增长的模式，因此注入后能量的提取是在自然起振能量提取前完成的，直观表现为脉冲建立时间的缩短。此外，由于良好的注入锁定所生成的脉冲的频率单一，因此观测到的脉冲图形较为光滑，而非注入锁定情况下生成的脉冲含有多种频率，因此观测到的脉冲波形图呈现调制状。通过增大注入种子光功率并精准控制 PZT，可以有效地提升注入锁定的效果。

在 Er∶YAG 激光器系统中，对于种子光与谐振光的耦合匹配，对注入锁定效果的主要影响因素为注入种子光与从动激光器的模式匹配。较长的注入光路、有限的空间以及凹面腔镜折返等多个因素均不利于模式匹配。

柱坐标系下的耦合系数[20]可以表示为

$$C_\omega=\frac{2}{\pi\omega_{10}\omega_{20}}\int_0^{2\pi}\int_0^\infty\exp\left(-\frac{\rho^2}{\omega_{10}^2}-\frac{\rho^2}{\omega_{20}^2}\right)\rho\,\mathrm{d}\rho\,\mathrm{d}\varphi, \tag{10}$$

式中：ω_{10} 和 ω_{20} 分别为谐振光与种子光的束腰半径；ρ 为径向距离；φ 为方位角。对(10)式指数项中的分母进行合并计算并积分得到

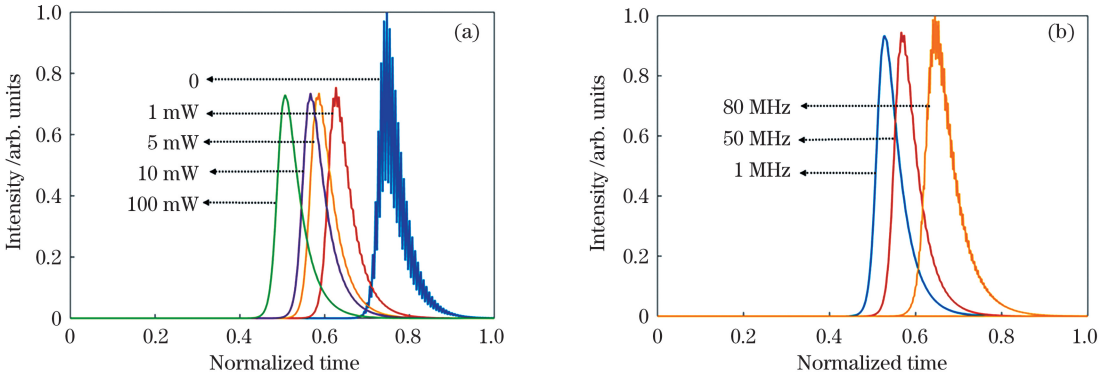

图 2　不同条件下的仿真脉冲波形图。(a)不同注入种子功率;(b) 不同频率失谐量

Fig. 2　Simulated pulse waveforms under different conditions. (a) Different injection seed powers; (b) different frequency detunings

$$C_{\omega}=\frac{2\omega_{10}\omega_{20}}{\omega_{10}^{2}+\omega_{20}^{2}}。\tag{11}$$

图 3 所示为不同 ω_{10} 下耦合系数与 ω_{20} 的关系的仿真结果。可以看出，$\omega_{10}=\omega_{20}$ 时耦合效率为 100%；ω_{10} 越大，两者间的束腰半径差对耦合效率的影响越小。根据实验条件计算可得，Er∶YAG 单频激光器系统中的种子光模式匹配耦合效率约为 80%。

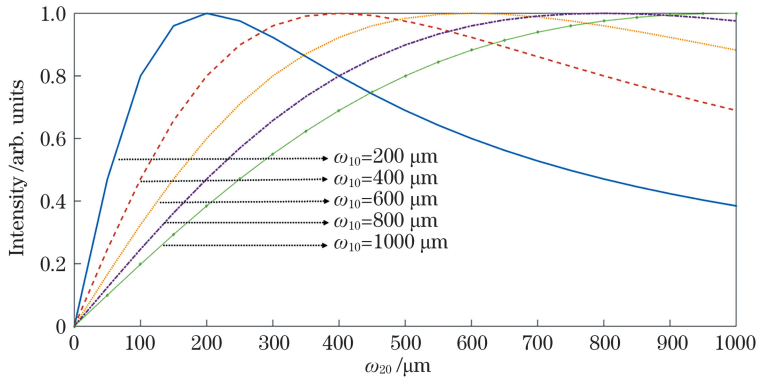

图 3　耦合系数与 ω_{20} 的关系的仿真结果

Fig. 3　Simulation results of relationship between coupling coefficient and ω_{20}

4　实验结果

当完成注入锁定后，激光器输出的是稳定的单频脉冲。在 200 Hz 的重复频率下进行了注入锁定的实验研究，得到单频脉冲能量和脉宽随入射泵浦功率的变化情况，如图4(a)所示，可以看出，最大脉

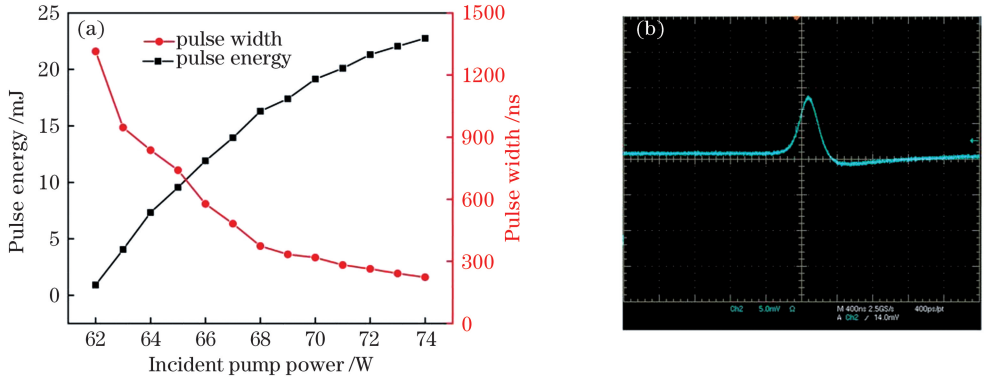

图 4　单频脉冲的能量和脉宽特性及波形图。(a)重复频率为 200 Hz 时，输出脉冲能量及脉宽随入射泵浦功率的变化曲线;(b)最大输出能量下的单频脉冲波形图

Fig. 4　Characteristics of energy and pulse duration as well as waveform diagram of single-frequency pulse. (a) Output pulse energy and pulse duration versus incident pump power at repetition frequency of 200 Hz; (b) waveform diagram of single-frequency pulse with maximum output energy

冲能量为 22.75 mJ，此时脉冲宽度为 223.1 ns。图 4(b)所示为最大输出能量下的单频脉冲波形图，种子注入后的脉冲只有一个纵模，因此包络变得十分光滑。

图 5(a)所示为最大能量下的外差拍频结果图，图 5(b)所示为拍频图的快速傅里叶变换结果。可以看出，输出激光脉冲为单频，外差信号的中心频率为 39.09 MHz，与声光移频量 40.68 Hz 近似；线宽为 2.46 MHz，是对应 223.1 ns 脉冲宽度下的傅里叶变换极限的 1.2 倍。

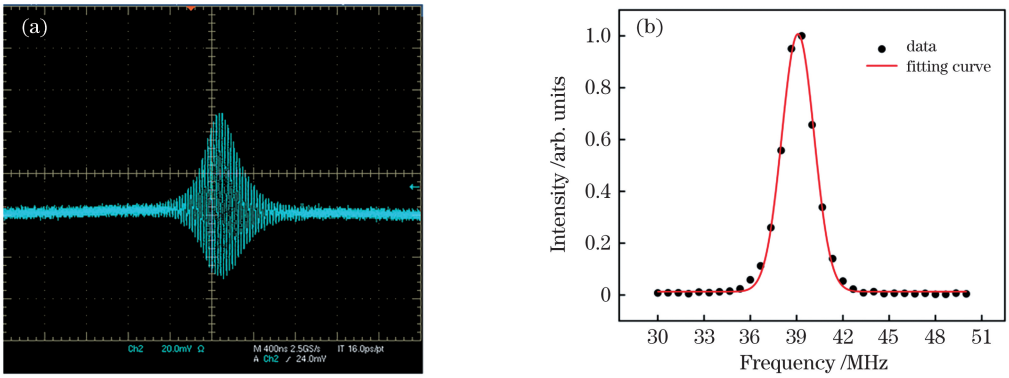

图 5　外差拍频测试结果。(a)外差拍频信号；(b)外差拍频信号的频谱

Fig. 5　Test results of heterodyne beat frequency. (a) Heterodyne beat signal; (b) spectrum of heterodyne beat signal

在激光脉冲输出能量最高的情况下测量 30 min 内的能量稳定性和频率稳定性，结果分别如图 6(a)、(b)所示。30 min 内能量抖动的标准差约为 0.118 mJ，频率漂移的标准差约为 0.578 MHz。

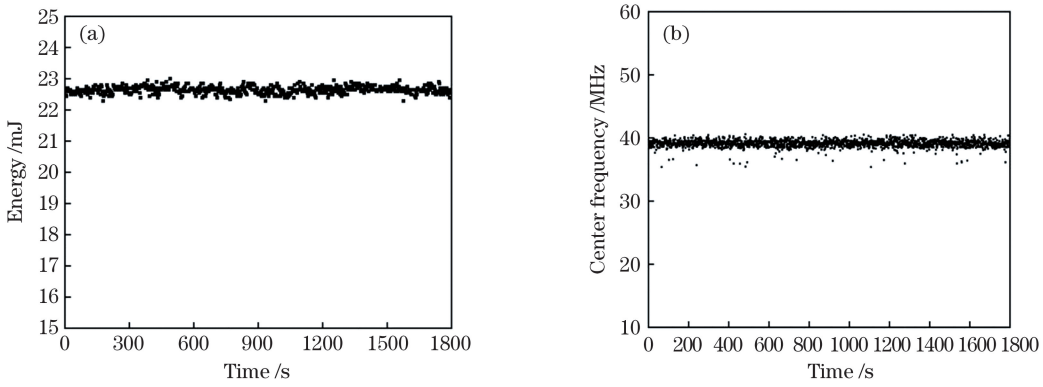

图 6　最高输出能量条件下 30 min 内的单频脉冲的稳定性测试结果。(a)能量稳定性；(b)频率稳定性；

Fig. 6　Stability test results within 30 min for single-frequency pulse with the highest output energy. (a) Energy stability; (b) frequency stability

利用红外相机测试最高输出能量下激光束腰附近不同位置处的光斑半径及光束质量因子，拟合结果如图 7 所示，x 方向的光束质量因子 M_x^2 和 y 方向的光束质量因子 M_y^2 分别为 1.16 和 1.15。

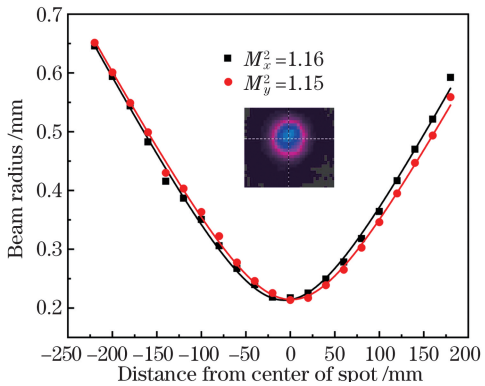

图 7　注入锁定模式下的激光光束质量

Fig. 7　Laser beam quality in injection locking mode

5　结　　论

研制了注入锁定双 Er∶YAG 陶瓷单频脉冲激光器系统，在重复频率为 200 Hz 的工作条件下获得了 22.75 mJ 的脉冲能量，对应的脉冲宽度为 223.1 ns。注入种子光后单频脉冲激光的光束质量因子在 x 和 y 方向上分别为 1.16 和 1.15。利用外差拍频技术得到单频调 Q Er∶YAG 激光器的脉冲频谱宽度为 2.46 MHz，是傅里叶变换极限的 1.2 倍。0.5 h 内的频率波动为 0.578 MHz，能量抖动为 0.118 mJ。这种性能稳定、结构紧凑的单频 Er∶YAG 脉冲激光系统可以为测风激光雷达和相干探测提供激光光源。

参 考 文 献

[1] Henderson S W, Hannon S M. Advanced coherent lidar system for wind measurements[J]. Proceedings of SPIE, 2005, 5887: 58870I.

[2] Stephan C, Alpers M, Millet B, et al. MERLIN: a space-based methane monitor[J]. Proceedings of SPIE, 2011, 8159: 815908.

[3] Stoneman R C, Hartman R, Schneider E A, et al. Eyesafe diffraction-limited single-frequency 1 ns pulsewidth Er∶YAG laser transmitter[J]. Proceedings of SPIE, 2007, 6552: 65520H.

[4] Chen Y J, Lin Y F, Huang J H, et al. Research progress in 1550-nm all-solid-state lasers based on Er^{3+}-doped crystals[J]. Chinese Journal of Lasers, 2020, 47(5): 0500018.
陈雨金, 林炎富, 黄建华, 等. 基于掺 Er^{3+} 晶体的 1550 nm 波段全固态激光研究进展[J]. 中国激光, 2020, 47(5): 0500018.

[5] Meissner A, Kucirek P, Li J, et al. Simulations and experiments on resonantly pumped single-frequency Erbium lasers at 1.6 μm[J]. Proceedings of SPIE, 2013, 8599: 85990H.

[6] Deng Y, Yu X, Yao B Q, et al. Single-frequency, *Q*-switched Er∶YAG at room temperature injection-seeded by an Er∶YAG nonplanar ring oscillator[J]. Laser Physics, 2014, 24(4): 045809.

[7] Gao C Q, Shi Y, Ye Q, et al. 10 mJ single-frequency, injection-seeded *Q*-switched Er∶YAG laser pumped by a 1470 nm fiber-coupled LD[J]. Laser Physics Letters, 2018, 15(2): 025003.

[8] Yao B Q, Deng Y, Dai T Y, et al. Single-frequency, injection-seeded Er∶YAG laser based on a bow-tie ring slave resonator[J]. Quantum Electronics, 2015, 45(8): 709-712.

[9] Burns P M, Chen M, Pachowicz D, et al. Single frequency Er∶YAG methane/water vapor DIAL source[C]// Applications of Lasers for Sensing and Free Space Communications, June 25-28, 2018, Orlando, Florida United States. Washington, D.C.: OSA, 2018: SW3H. 2.

[10] Shi Y, Gao C, Wang S, et al. High-energy, single-frequency, *Q*-switched Er∶YAG laser with a double-crystals-end-pumping architecture[J]. Optics Express, 2019, 27(3): 2671-2680.

[11] Lin W P, Jiang N, Zhou T J, et al. 1030 nm laser amplification of Yb∶YAG ceramic planar waveguide[J]. Chinese Journal of Lasers, 2019, 46(5): 0501002.
林伟平, 姜楠, 周唐建, 等. Yb: YAG 陶瓷平面波导 1030 nm 激光放大[J]. 中国激光, 2019, 46(5): 0501002.

[12] Yang H L, Chen Y, Jia F Q, et al. Research progress in ceramic lasers[J]. Laser & Optoelectronics Progress, 2020, 57(7): 071610.
杨昊霖, 陈玥, 贾富强, 等. 陶瓷激光器研究进展[J]. 激光与光电子学进展, 2020, 57(7): 071610.

[13] Ye Q, Gao C Q, Wang S, et al. Single-frequency, injection-seeded *Q*-switched operation of resonantly pumped Er∶YAG ceramic laser at 1645 nm[J]. Applied Physics B, 2016, 122(7): 1-5.

[14] Wang S, Shi Y, Li S H, et al. Diode-pumped single-frequency Er∶YAG ceramic pulsed laser[J]. Acta Optica Sinica, 2018, 38(9): 0914003.
王硕, 史阳, 李尚桦, 等. 半导体抽运的 Er∶YAG 陶瓷单频脉冲激光器[J]. 光学学报, 2018, 38(9): 0914003.

[15] Li S, Wang Q, Song R, et al. Laser diode pumped high-energy single-frequency Er∶YAG laser with hundreds of nanoseconds pulse duration[J]. Chinese Optics Letters, 2020, 18(3): 031401.

[16] Zhang M, Gao C Q, Gao M W, et al. 16 W single-frequency laser output from an Er∶YAG ceramic nonplanar ring oscillator[J]. Laser Physics Letters, 2018, 15(12): 125803.

[17] Park Y, Giuliani G, Byer R. Single axial mode operation of a *Q*-switched Nd∶YAG oscillator by injection seeding[J]. IEEE Journal of Quantum Electronics, 1984, 20(2): 117-125.

[18] Degnan J J. Theory of the optimally coupled *Q*-switched laser[J]. IEEE Journal of Quantum Electronics, 1989, 25(2): 214-220.

[19] Cao X Z, Li P L, Liu Q. Theoretical and experimental investigation of injection seeded Nd∶YAG zigzag slab ring lasers[J]. Optics & Laser Technology, 2020, 123:105912.

[20] Wu C T, Chen F, Dai T Y, et al. Theoretical and experimental investigations of injection-locked signal extraction of Tm: YAG laser[J]. Journal of Modern Optics, 2015, 62(19): 1535-1545.

1645-nm Single-Frequency Pulsed Er∶YAG Ceramic Laser

Song Rui, Li Shanghua, Chen Chaoyong, Wang Qing, Gao Mingwei, Gao Chunqing*

MOE Key Laboratory of Photoelectronic Imaging Technology and System, School of Optics and Photonics, Beijing Institute of Technology, Beijing 100081, *China*

Abstract

Objective Stable single-frequency and high-energy lasers in the eye-safe band are important light sources for lidars and coherent detection. Currently, many studies have reported a human eye-safe 1645-nm single-frequency pulsed laser output. Er∶YAG crystals and Er∶YAG ceramics are two main types of common-gain media for realizing 1645-nm lasers. Compared with crystalline materials, ceramic materials possess the advantages of short growth time, large-scale production, and flexible doping concentration. In the present study, we report the results of an engineered prototype of a single-frequency pulsed Er∶YAG ceramic laser. The volume of this laser system is reduced, and the frequency stability is improved. An optimized symmetrically pumped double Er∶YAG ceramic structure is designed to solve the problem of performance degradation caused by limited space. Such a single-frequency laser light source with a smaller volume and higher stability is more helpful for a practical application.

Methods The single-frequency Er∶YAG pulsed laser system with seed injection mainly includes three parts: an Er∶YAG master laser, a symmetrically pumped dual Er∶YAG ceramic ring-cavity slave laser, and a detection-control system. To improve the stability of the pulsed laser, a single-frequency continuous Er∶YAG non-planar ring-cavity laser is employed as a master laser. To improve the mode-matching efficiency and reduce the laser volume, the slave-laser cavity is designed with a multiple-folding structure that adopts total reflecting mirrors. This structure is a symmetrical one of dual laser-diode (LD)-pumped dual Er∶YAG ceramics. To simultaneously satisfy the requirements of pulse energy and pulse width for lidars, the total cavity length is set to 2.3 m. By using multiple folding mirrors, the volume of the cavity is reduced, and a space is reserved for the seed laser at the center position to realize a reasonable use of space. The working process of the seed injection and laser output is described as follows: a p-polarized seed light is reflected by the injection mirror and enters the slave-laser cavity. The seed laser is then injected through the path of the first diffraction order of the acousto-optic modulator (AOM). In this manner, resonance is realized in the slave laser, and the AOM shuts off the optical path during this period. The photodetector detects the leaked resonant signal and transmits it to the control system. Simultaneously, the control system loads a triangular wave to the piezoelectric ceramic (lead zirconate titanate) to allow it to continuously scan the cavity length. When the peak of the resonant signal has been scanned, the AOM is stopped from turning off the optical path to establish the laser pulse.

Results and Discussions The realization of the stable single-frequency laser output with seed injection is shown. An experimental study of the injection-locked laser is conducted at a repetition rate of 200 Hz. The energy and pulse duration of the single-frequency laser linearly change with the increase in the incident pump power [Fig. 4(a)]. The obtained maximum pulse energy is 22.75 mJ, and the corresponding pulse duration is 223.1 ns. The envelope of the single-frequency pulsed waveform becomes very smooth [Fig. 4(b)] because only one longitudinal mode is present in the pulse after the seed injection. The heterodyne beat-frequency technique is used to detect the single-frequency characteristics of the obtained pulsed laser. The heterodyne beat frequency is obtained at the maximum output energy [Fig. 5(a)], and a fast Fourier transform is performed on the beat-frequency result [Fig. 5(b)]. The spectrogram shows that the output laser pulse has a single-frequency, and the center frequency of the heterodyne signal is 39.09 MHz, which is similar to the acousto-optic frequency shift of 40.68 Hz. The full width at half maximum of the spectrum is 2.46 MHz, 1.2 times the Fourier transform limit, which corresponds to a pulse duration of 223.1 ns. We measure the energy and frequency stabilities when the output energy of the laser pulse is kept at the highest level. The standard deviation of the energy jitter within 30 min is approximately 0.118 mJ [Fig. 6(a)], and the standard deviation of the frequency drift is approximately 0.578 MHz [Fig. 6(b)]. The spot-radius values of the pulsed laser with the highest energy are recorded using an infrared camera at different positions. Subsequently, the results are fitted and calculated, and the beam quality factors in the x and y directions are 1.16 and 1.15, respectively (Fig. 7).

Conclusions In this study, a single-frequency laser is designed and developed based on the seed-injection technology, in which the dual Er∶YAG ceramic symmetrical structure is end-pumped by a dual 1470-nm LD. Through the theoretical analysis, it is found that the main factors determining the seed-injection effect are the coupling of the seed with oscillating lasers, the power, and the frequency detuning of the seed laser. In the experiment, the obtained maximum average pulse energy is 22.75 mJ at a repetition rate of 200 Hz, and the corresponding pulse duration is 223.1 ns. The beam quality factors of the single-frequency pulsed laser are 1.16 and 1.15 in the x and y directions, respectively. The spectral width of this Q-switched single-frequency laser is 2.46 MHz and is 1.2 times of the Fourier transform limit. The standard deviation of the energy jitter is 0.118 mJ, and the standard deviation of the center frequency drift is 578 kHz. This stable and compact single-frequency Er∶YAG pulsed laser system can be used as a laser source for wind lidar and coherent detection.

Key words lasers; all-solid-state lasers; injection locking; high energy; single frequency; laser ceramics

OCIS codes 140.3460; 140.3538; 140.3480